Microchemical Journal 213 (2025) 113756

Contents lists available at ScienceDirect

Microchemical Journal

journal homepage: www.elsevier.com/locate/microc

A comparative analysis of elemental imaging of marine mollusc shells using Laser Induced Breakdown Spectroscopy

Jesús Mirapeix [a,e,*], Rosa Arniz-Mateos [b,c], Danai Theodoraki [b], Asier García-Escárzaga [d], Víctor Piñon [f], Igor Gutierrez-Zugasti [c], Niklas Hausmann [b], Adolfo Cobo [a,c,e]

[a] Photonics Engineering Group, Universidad de Cantabria, Santander, Spain
[b] Leibniz Zentrum für Archäologie (LEIZA), Mainz, Rhineland-Palatinate, Germany
[c] Instituto Internacional de Investigaciones Prehistóricas de Cantabria (Universidad de Cantabria, Gobierno de Cantabria, Grupo Santander), Santander, Spain
[d] Department of Prehistory and Institute of Environmental Science and Technology (ICTA), Universitat Autònoma de Barcelona, Bellaterra, Spain
[e] CIBER de Bioingeniería, Biomateriales y Nanomedicina (CIBER-BBN), Instituto de Salud Carlos III, Madrid 28029, Spain
[f] Institute of Electronic Structure and Laser (IESL), Foundation for Research and Technology-Hellas, N. Plastira Str. 100, 70013 Heraklion, Crete, Greece

ARTICLE INFO

Keywords:
LIBS
Elemental analysis
Archaeology
Mollusc shells
Comparative analysis
Paleoclimate

ABSTRACT

The elemental composition of marine mollusc shells can offer valuable information about palaeoclimate and the season of shell collection. In particular, the correlation between Mg/Ca ratios of shell carbonate and the sea surface temperature has been tested. However, this correlation can also be strongly dependent on endogenous mechanisms of the animals. These mechanisms are still poorly understood and are often difficult to distinguish from methodological effects. Here we present the results of a comparative study of LIBS analyses performed on modern limpet (*Patella vulgata* Linnaeus, 1758) shells in two different laboratories (UC-PEG and LEIZA). In particular, 2D LIBS imaging has been performed to obtain the associated elemental composition in an attempt to avoid the uncertainties derived from the use of linear scanning trajectories on the shells. The goal of this study is to evaluate the impact of the different setups and processing techniques employed on the obtained results regarding palaeoclimatic information and the possible implications in the interpretation of these data. We demonstrate that the uncertainties found in the analysis of some of the specimens are not related to the specifics of the LIBS technique, but to the irregularity of limpet growth patterns themselves.

1. Introduction

The study of marine mollusc shells has long been an essential avenue for investigating past environmental conditions, ranging from sea surface temperature (SST) to salinity and marine productivity [1-3]. These shells provide high-resolution records that can be accessed through microscopic and chemical analyses, a field known as sclerochronology. These analyses have been primarily focused on the use of stable oxygen isotope ratios ($^{18}O/^{16}O$, with values expressed in $\delta^{18}O$) given their potential to act as a powerful proxy for past SST [4-8]. Even if it has been successfully applied to the study of mollusc shells, there are some limitations related to this method, due to the expensive and time-consuming sampling and analytical procedures that are required [9,10].

The analysis of the variations in elemental ratios (e.g., Mg/Ca, Sr/Ca, Ba/Ca) offers a promising alternative solution in this context, as several studies have established a relationship between the substitution rate of these elements and the SST [11-14]. Typically, Mg/Ca ratios and their spatial variation within shell carbonate have been assessed by means of Laser Ablation-Inductively Coupled Plasma-Mass Spectrometry (LA-ICP-MS) [14] or Inductively Coupled Plasma-Optical Emission Spectrometry (ICP-OES) [15-17]. These methods, while highly accurate, are also time-consuming, requiring an initial stage of sample preparation, and often resource-intensive. Thus, fast and more cost-effective methods of analysis can be of particular interest for this initial step of establishing environmental proxies. The analysis of mollusc shells holds broad relevance beyond palaeoclimatic reconstruction. Due to their widespread presence in archaeological sites, chronological resolution at sub-seasonal scales, and sensitivity to environmental variation, mollusc shells serve as valuable bioarchives in both environmental and archaeological research. Their geochemical composition can reveal past sea surface temperatures, seasonality of resource use, and environmental stress events—offering critical insights into human-environment

* Corresponding author at: Photonics Engineering Group, Universidad de Cantabria, Santander, Spain.
E-mail address: jesus.mirapeix@unican.es (J. Mirapeix).

https://doi.org/10.1016/j.microc.2025.113756
Received 12 February 2025; Received in revised form 1 April 2025; Accepted 23 April 2025
Available online 24 April 2025

dynamics, mobility, and subsistence strategies in coastal societies [1,8,9,18-22].

In this context, Laser-Induced Breakdown Spectroscopy (LIBS), emerges as a promising alternative. LIBS offers distinct advantages, including high-speed operation, minimal sample preparation, and the ability to perform *in situ* measurements [23]. In brief, this technique operates by focusing high-energy laser pulses on the sample, which gives rise to a material ablation and plasma generation. This plasma emits light and the measured spectrum is formed by emission lines associated with the different chemical species participating in the process. The information provided by these lines enables the estimation of the elemental concentration of the sample. LIBS has already been studied for the estimation of Mg/Ca ratios of marine mollusc shells from different areas such as the Atlantic Ocean and Mediterranean Sea and different species, such as *Phorcus lineatus* (da Costa, 1778) [24], *Patella vulgata* Linnaeus, 1758 [25,26], *Patella caerulea* Linnaeus, 1758 [27] and *Patella depressa* Pennant, 1777 [28,29], among others [30-33]. In these previous works, Mg/Ca ratios have been estimated from simple two emission line ratios [25,26] or calculated as molar ratios using the Calibration-free LIBS (CF-LIBS) algorithm [28]. The traditional approach in this regard has been to define a linear trajectory from the most recent growth increment at the shell edge to the apex going through approximately the middle of the m + 2 calcite layer to avoid parts along the outer shell edge with occasional Mg/Ca anomalies [27]. While the use of linear trajectories following the direction of growth within a shell layer has been the common approach, it is susceptible to endogenous factors affecting the environmental analysis [4]. In fact, endogenous mechanisms, often species-specific or even specimen-specific, have added a layer of difficulty to the interpretation of shell chemistry [34]. For instance, variations in the elemental composition of growth increments have been attributed to differences in the crystal fabric, such as changes in crystal size and orientation [34,35]. Some authors have also explored variations in shell chemistry within and between species, for example analysing the differences found in specimens of the same species but collected at different geographical locations, or even between specimens of the same species sharing the same location [6,36]. This highlights the challenges and complexities of interpreting data provided by the analysis of elemental ratios in the context of mollusc shells.

As an alternative to the analysis based on linear trajectories, 2D elemental imaging of whole shell sections or surfaces have also been performed [13,27,32,37], following the use of 2D elemental mapping via LIBS in other applications like the generation of chemical maps of paper coatings or photovoltaic cells [38], rare earth samples [39] or the determination of shooting distance in forensic laboratories [40]. 2D elemental maps provide a means to navigate the potentially complex interplay between environmental and endogenous factors, as it detects variations in the Mg/Ca ratios along isochronous growth increments. However, because the origin of elemental anomalies is not always obvious and cannot consistently be associated with endogenous factors, they could also be explained by experimental parameters or setup of the employed LIBS system itself. LIBS is known to be sensitive to experimental parameters, with factors such as laser defocusing and temporal resolution significantly influencing the results. Matrix effects, i.e., the influence of general chemical and physical variations in the sample on the estimated concentration of a particular element, are also an issue. These matrix effects can vary in their impact depending on the experimental conditions, making it crucial to optimise parameters for specific analyses in particular matrices. Additionally, the laser-material interaction involves complex nonlinear processes that are not fully understood, further complicating the prediction of the optical emission and therefore the concentration estimates. These factors collectively challenge the reproducibility and quantitative accuracy of LIBS measurements in different laboratories [32].

LIBS has been previously applied to analyse elemental compositions in marine mollusc shells [18-28], but our study presents several novel contributions to the field. First, we provide the first inter-laboratory comparison of LIBS measurements on identical shell specimens, addressing a critical gap in understanding methodological reproducibility across different research settings. Previous studies have typically relied on data from a single laboratory setup, leaving questions about the consistency of LIBS results across different systems unaddressed: in this study results from the Emmy-Noether-Group Seafront of Leibniz Zentrum für Archäologie (LEIZA) in Mainz, Germany [41]; and Photonics Engineering Group (PEG) of Universidad de Cantabria (UC) at Santander, Spain, will be compared and discussed. Second, our approach specifically aims to differentiate between anomalies in 2D elemental maps that are attributable to the LIBS technique itself versus those that represent genuine biological or environmental signals. This distinction is crucial for improving the reliability of LIBS as a paleoenvironmental proxy tool. Finally, by systematically examining *P. vulgata* shells using two independent LIBS systems with different configurations, we establish a methodological framework for distinguishing inherent sample characteristics from instrumental artifacts, a challenge that has not been comprehensively addressed in previous geochemical applications of LIBS. These contributions collectively advance the application of LIBS technology in paleoclimatic and archaeological research by enhancing our understanding of the intricate relationships between environmental changes and mollusc shell composition.

We aim to assess whether anomalies in the elemental maps, that are not explained by environmental factors, occur consistently on elemental maps from both systems or are restricted to each system only. Furthermore, we aim to address how this uncertainty hinders researchers in determining areas of interest in palaeoclimatic and archaeological research. By comparing the results obtained from two different laboratories, we aim to establish that these divergences are not related to the LIBS technique but to a complex interplay of various factors inherent to the sample material. This comparative approach allows us to contribute to a deeper understanding of the intricate relationships between environmental changes and mollusc shell composition.

2. Materials

Our study was performed using an assemblage of 20 shells of *P. vulgata* collected in Langre Beach (Cantabria, Spain) in 2012. The analysis has been focused on *P. vulgata* shells because this taxon, commonly found on the rocky shores of Atlantic Europe [42], presents a valuable model for archaeological investigations [26,43-45]. The complete set is uniformly distributed among the four different seasons with 5 specimens per season each to be analysed at LEIZA and PEG laboratories. The morphology of the shells was considered during the collection program, with the aim of selecting specimens from lower zones that remain submerged for longer periods. This makes it more likely that these shells experienced regular growth avoiding stops [46,47]. Table 1 presents biometrical and weight information from the shells under analysis and Figs. 1 and 2 show the geographical location where the specimens were collected. SST (daily average) recorded from El Bocal station (Santander), property of the Instituto Español de Oceanografía (http://www.ieosantander.net/), and located ca. 11 km away from the site of collection were 14.6 °C (12 November 2011), 11.7 °C (23 February 2012), 15.2 °C (3 June 2012) and 20.8 °C (5 August 2012).

The preparation of the shells for the analysis followed an established procedure of sectioning in parallel to the maximum growth axis [32] using a low-speed Bruehler Isomet 1000 saw with a 0.5 mm wide diamond blade and a minimal cutting speed of 100 rpm, employing a water-cooling process to prevent overheating or structural damage on the surface of the shell. The samples were also polished with Silicon carbide SiC powder with grains of 600 and 800 mg and with with aluminum oxide (Al_2O_3) with a 1 μm thickness, for 5 min each step, in order to clean the surface. The possible appearance of impurities was monitored during the LIBS scanning processes, for example by checking the intensity of the Si I emission line at 288.16 nm, thereby ensuring that no interference occurred.

Table 1
Biometrical and weight information from the 20 specimens of *P. vulgata* collected in Langre Beach (Cantabria, Spain) between November 2011 and August 2012. The sample identification consists of the abbreviation LAN (Langre) and a unique increasing number.

Sample ID	Length (mm)	Width (mm)	Height (mm)	Weight (g)	Date of collection
LAN96	21.32	24.20	11.20	2.0	12 November 2011
LAN98	24.55	20.12	10.86	1.4	12 November 2011
LAN100	30.57	25.88	14.26	3.4	12 November 2011
LAN105	27.47	22.44	10.48	1.5	12 November 2011
LAN109	32.58	27.48	14.37	2.8	12 November 2011
LAN176	27.80	22.90	11.30	1.7	23 February 2012
LAN177	34.50	28.50	13.30	3.7	23 February 2012
LAN182	33.80	27.40	11.20	2.9	23 February 2012
LAN183	27.90	22.90	13.20	2.0	23 February 2012
LAN184	31.80	26.90	10.60	2.0	23 February 2012
LAN229	32.00	25.30	13.80	2.5	3 June 2012
LAN230	31.80	24.40	13.90	2.5	3 June 2012
LAN231	34.10	29.10	15.50	3.7	3 June 2012
LAN235	31.10	25.30	14.10	2.3	3 June 2012
LAN236	32.50	26.50	13.90	2.7	3 June 2012
LAN237	31.60	25.40	11.40	1.9	3 June 2012
LAN254	31.10	26.80	13.60	2.8	5 August 2012
LAN255	32.40	26.00	13.30	3.3	5 August 2012
LAN256	28.50	23.50	13.20	1.9	5 August 2012
LAN258	33.50	27.60	13.30	2.8	5 August 2012

3. Methods

3.1. Experimental setups

The two laboratories use different LIBS systems (Fig. 3). The LIBS system of the LEIZA laboratory, developed by IESL-FORTH, employs a Litron Nano DPSS 60–100 laser with an operating wavelength of 1064 nm. This laser emits pulses of 8 ns duration with an energy of 1.4 mJ, and is focused directly on the sample using a x10 microscope objective (Thorlabs) [23]. The light emitted in this process is captured by a 600 μm diameter optical fibre, which is coupled to an Andor Kymera 193-A spectrometer and an Andor ICCD iStar DH320T-25F-03 detector for signal intensification. It is equipped with a 1800 l/mm grating resulting in a 0.06 nm/pixel resolution and a spectral range of ~ 65 nm. An internal delay generator sets the delay time to 0.5 μs and the integration time to 1 μs. The laser is contained in a beam tube that is directed into the sample chamber, which contains a motorised platform in XYZ. In addition, it has a camera for sample visualisation and a laser distance sensor for precise z-axis positioning. The system software allows linear scans and 2D maps to be drawn. The sampling speed depends on the resolution with 0.20 s per point acquisition at 100 μm and 0.13 s per point (or ~ 5 and ~ 8 points per second, respectively). A maximum of 20,000 points per run can be programmed. Linear trajectories consisting of 200–500 points are made in a matter of seconds, and 2D maps (3,000–6,000 points) are generated in about fifteen to thirty minutes.

The setup used at PEG is formed by a laser source [Q-Switched Nd:YAG double-pulsed laser, (Lotis LS-2134D)] operating at 1064 nm with a 10 Hz rate and using 16 ns pulses and a pulse energy of approximately 35 mJ. The laser light is focused by means of a x10 objective, giving rise to a laser spot of 100 μm. Once the plasma is formed over the specimen surface, its light is collected by a system composed of a collimating lens and a fused silica, solarization resistant, 1 mm core diameter optical fibre. This fibre is coupled to a bundle of eight 200 μm core diameter optical fibres, which deliver the light to an eight-channel Avantes ULS2048-USB2-RM CCD spectrometer. Its spectral range covers from 178 to 889 nm, with a resolution between 0.015 and 0.06 nm.

The stability of both systems during the experiments is guaranteed by controlling the ambient temperature. The spectrometer used at LEIZA is calibrated before each measurement and any possible wavelength shift due to ambient temperature during measurements is negligible. In addition, the algorithm employed in the data processing to calculate the emission lines ratios accounts for any possible shifts in the peak positions. The spectrometer used at PEG is a CCD-based system with no moving parts and exhibits very good long-term stability; nevertheless, it is periodically recalibrated. Additionally, the spectral processing algorithm actively searches for and models the emission peaks, ensuring that any potential wavelength shift due to spectrometer miscalibration would be automatically detected. The pulse energy stability of both lasers (PEG and LEIZA) is better than 1 %, having virtually no impact on the plasma properties or the ablation process.

Table 2 presents a comparison of the values of the main parameters selected at each laboratory.

3.2. Processing techniques

Apart from the different experimental setups, it is worth noting that the techniques employed to obtain the raw Mg/Ca ratio data have also been different between the two research groups. The LEIZA group has directly used the ratio of two emission lines: Ca II at 315.887 nm and Mg II at 279.553 nm. The selection of these lines is performed taking into account the spectral range offered by the chosen spectrometer, the lines (in particular the Ca line) providing the highest available intensity and considering that both lines had to be generated from transitions of the same state of ionisation [48]. The processing of the spectral analysis shows the average values of the Mg/Ca line intensity ratio, ranging between approximately 0.04 and 1.

The results obtained by PEG are derived from the use of the Calibration-Free LIBS (CF-LIBS) methodology [28], thus producing 2D maps of Mg/Ca molar concentration. CF-LIBS [49] enables the generation of quantitative measurements of the elemental composition of the sample under analysis without using calibration curves and allowing to overcome the matrix effect. To apply this method, certain assumptions about plasma conditions must be satisfied. Specifically, it is assumed that (1) ablation is stoichiometric, meaning that the plasma composition reflects that of the original sample; (2) the plasma is in local thermodynamic equilibrium (LTE) within the observation window; and (3) the plasma is optically thin, so that self-absorption of emission lines is negligible. Additionally, the spectral range must include identifiable emission lines for all elements present in the sample [50]. Given that a non-gated spectrometer is used in the LIBS setup at PEG, verifying LTE conditions is especially important, as the time integration window exceeds the plasma lifetime and only the delay relative to the laser pulse can be precisely adjusted. LTE is generally favoured when collisional processes dominate over radiative ones (early plasma evolution) and when thermodynamic parameters remain relatively constant (late stages). A delay of 1 μs after the laser shot was chosen, a value commonly adopted in CF-LIBS studies [50]. This delay offers reduced continuum background and sufficiently intense atomic emissions, providing an effective “gated-like” behaviour due to the rapid decay of the plasma. Experimental measurements showed that the Ca I and Mg I lines decreased to 10 % of their peak intensity approximately 6 μs after the pulse, while Ca II and Mg II lines disappeared after approximately 2 μs. This indicates that with a 1 μs delay, the effective capture window is approximately 5 μs, supporting the LTE condition and enabling accurate CF-LIBS analysis under these settings [51].

Selecting appropriate emission lines is another key step in the application of CF-LIBS, as they are used in the Saha-Boltzmann plots, which are essential for determining the plasma temperature, electron

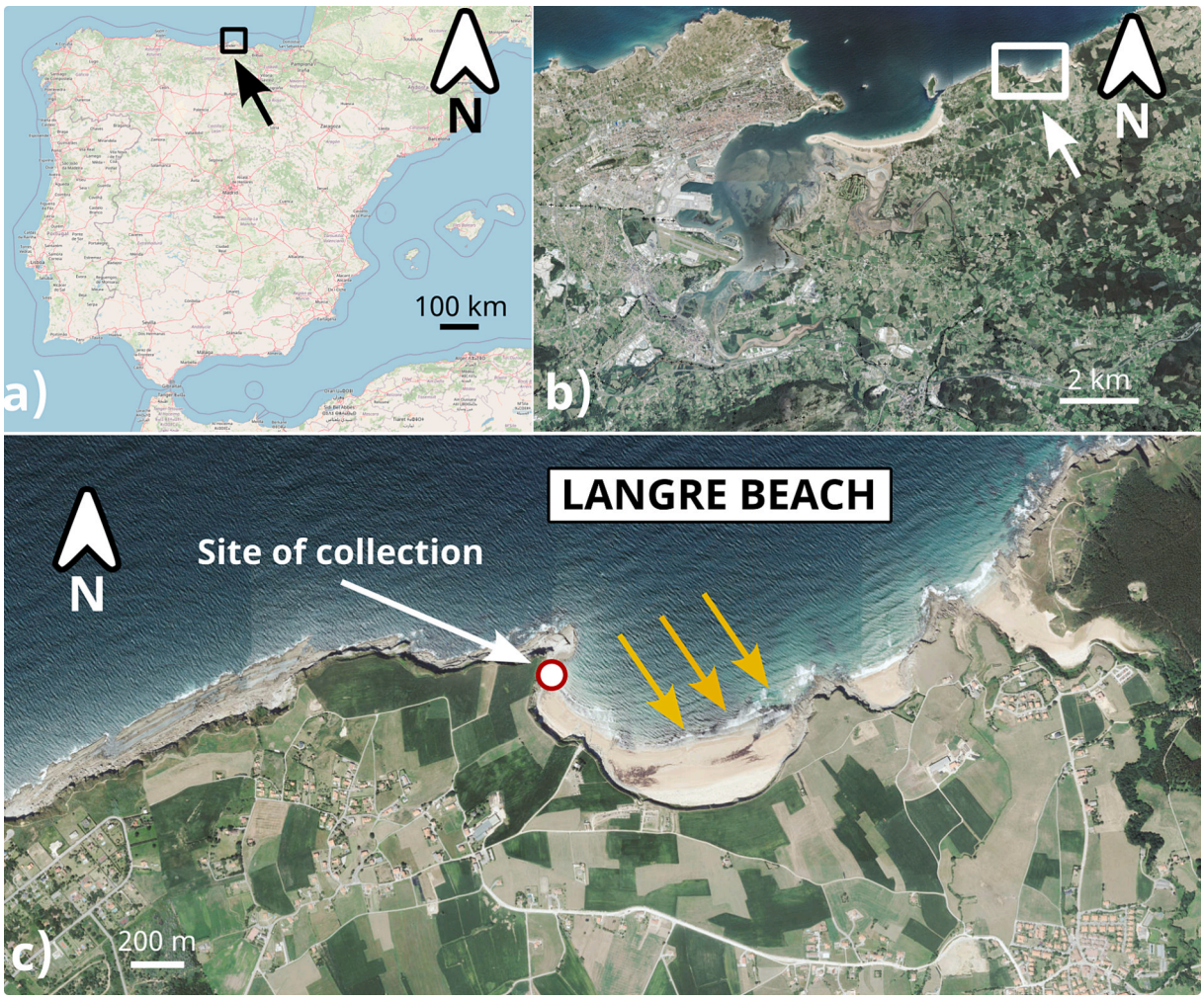

Fig. 1. Location of the site of collection: (a) detail of the location on the map of the Iberian Peninsula; (b) location in detail of Langre Beach on the open coast of the Cantabrian Sea, near the city of Santander (on the top-left part of the image); (c) detail of Langre Beach at Ribamontán al Mar (Cantabria), yellow arrows indicate the regular direction of waves. (a) The image was created using data from OpenStreetMap, which is freely available under the Open Database License (ODbL); (b) and (c) were created using data from the Government of Cantabria (https://mapas.cantabria.es). (For interpretation of the references to colour in this figure legend, the reader is referred to the web version of this article.)

density, and elemental concentration. To ensure that only optically thin emission lines were used in the CF-LIBS algorithm, a systematic selection process based on recommendations by Hongbo et al. [52] was implemented. The procedure began with an analysis of the average spectrum derived from all measurements for each sample, followed by comprehensive line identification. We established selection criteria focusing on multiple parameters: line intensity, signal-to-background ratio, overlapping with lines of identical or different species, and isolation from other lines. For emission lines that met these initial requirements, their spectroscopic characteristics are obtained from NIST [48] and Genie databases [53]. The Ca and Mg emission lines used for the analysis in this work are presented in Table 3. It should be noted that an additional important criterion in our application is that the selected lines should be available in all spatial points of the shell. In this way, each Saha-Boltzmann plot will be created with the same number of lines, helping to reduce the variability of the ratio sequences.

It is also worth noting that, as detailed in Table 2, different laser pulse durations have been used at LEIZA and PEG (8 and 16 ns, respectively). Provided that the resulting Mg/Ca ratios have been obtained using the ratio of two emission lines and the CF-LIBS approach and both methods are robust against variations in laser parameters as they rely on normalized spectral information rather than absolute intensities, this difference is expected to have a negligible effect on the 2D LIBS maps obtained for each specimen.

Ten shots are taken per point at both laboratories during the mapping process via LIBS, with the spectra being treated by omitting the first 3 (LEIZA) or 5 (PEG) out of every 10 obtained per point and counting them as cleaning shots. The remaining 7 (LEIZA) or 5 (PEG) spectra are accumulated and considered for the generation of the corresponding elemental information. A diameter of 20 μm and a distance of 100 μm between each point along the entire growth of the shell or 30 μm distance in smaller areas at the anterior and/or posterior side of the shell are considered at LEIZA, while a spatial resolution of 50 μm is used during the measurements performed at PEG.

As an example of the procedure followed to obtain the 2D LIBS maps of the Mg/Ca ratios, Fig. 4 shows the results derived from the analysis carried out at LEIZA of the specimen LAN182 (*P. vulgata*) collected in February 2012.

In Fig. 4, the sections with higher Mg/Ca ratios are visible in lighter colours (according to the colour scale associated with the Mg/Ca ratio) in Fig. 4(a), (b1) and (c1). The associated Mg/Ca evolution profiles, presented in Fig. 4(b2) and (c2), have been directly calculated as the ratios of the previously mentioned Mg and Ca emission lines following the black dashed line indicated on the 2D map, where DoG indicates the direction of growth. The 2D map of the posterior side of the shell has been rotated to allow a better comparison with the corresponding Mg/

Fig. 2. Image of the site of collection at Langre Beach (Ribamontán al Mar, Cantabria, Spain).

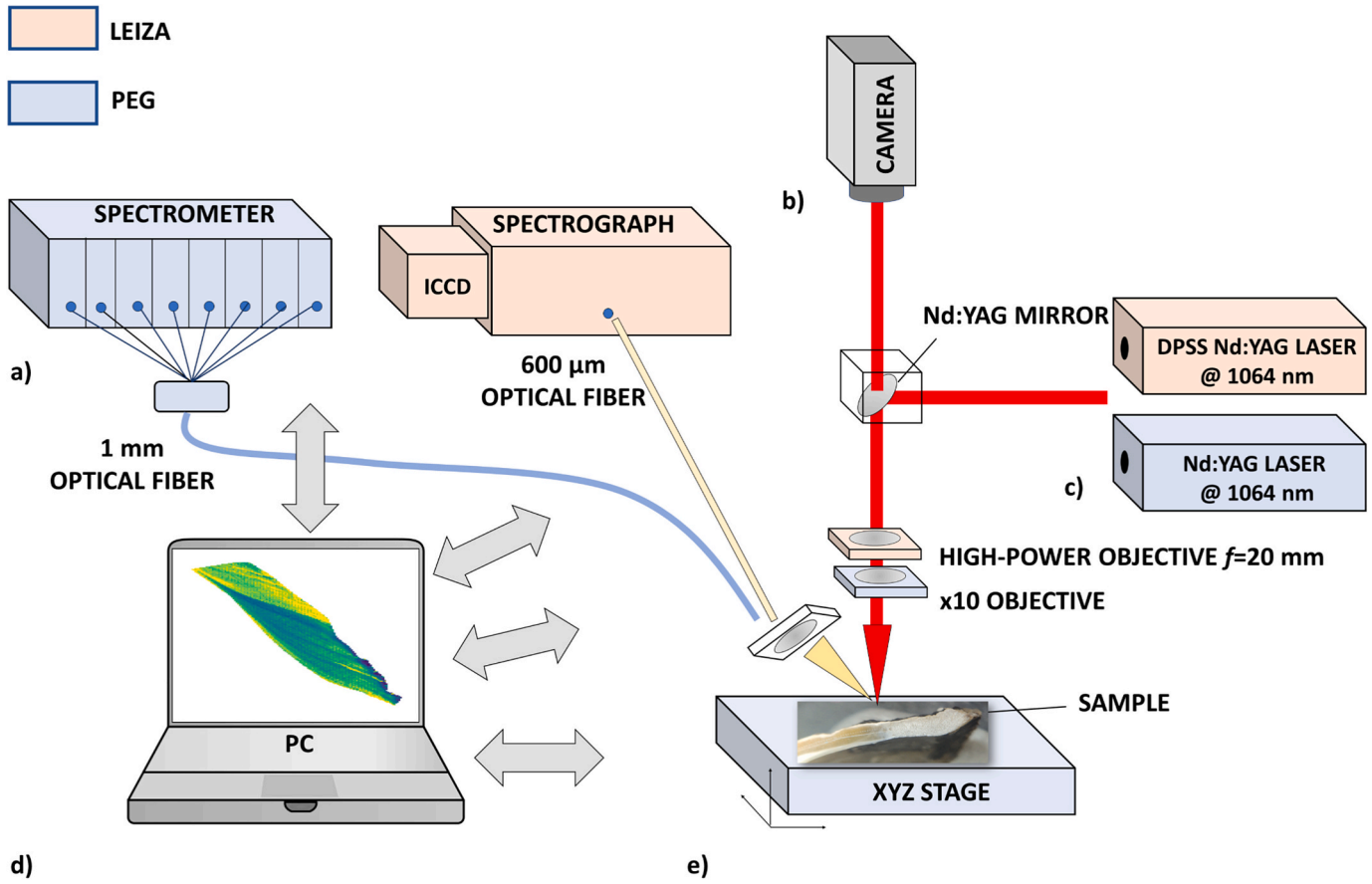

Fig. 3. Schematic diagram of the LIBS setups employed at LEIZA (Mainz, Germany) and PEG (Santander, Spain): (a) spectrometers; (b) camera for sample visualisation; (c) laser sources; (d) PC for setup control (grey arrows indicate communications with the other devices) and processing; (e) XYZ motorised platform.

Table 2
Comparison of the values of the main parameters associated with the LIBS setups at LEIZA and PEG laboratories.

	LEIZA	PEG
Laser model	Litron Nano DPSS 60-100	Q-Switched Nd:YAG double-pulsed (Lotis LS-2134D)
Laser wavelength (nm)	1064	1064
Laser frequency (Hz)	100	10
Laser pulse duration (ns)	8	16
Laser pulse energy (mJ)	1.4	35
Spatial resolution (μm)	30	50
Number of pulses per point	7	5
Delay time (μs)	0.5	1
Spectrometer model	Andor Kymera 193-A spectrometer	Avantes ULS2048-USB2-RM
Spectrometer spectral range	267.5–332.5	178 – 889
Spectrometer resolution (nm)	0.06	0.06
Optical fiber diamenter (mm)	0.6	1
Focusing optics	High-power objective f = 20 mm	X10 objective
Processing method	Ratio of 2 emission lines	CF-LIBS
Measurement time (minutes)	15–30	150–200

Table 3
Spectroscopic information of the Ca and Mg atomic lines employed in the CF-LIBS calculations, with the atomic lines used in simple intensity ratio calculations in bold. Data from the NIST Atomic Spectra Database [48].

Element	Ionisation	Wavelength (nm)	A_{ki} (s^{-1}) × 10^8	g_k	E_k (eV)	k_t
Ca	I	227.55	0.30	3	5.45	11.11
Ca	I	239.86	0.17	3	5.17	7.61
Ca	I	558.20	0.06	7	4.74	5.63
Ca	**II**	**315.89**	**3.10**	**4**	**7.05**	**7.45**
Ca	II	370.60	0.88	2	6.47	1.98
Ca	II	373.69	1.70	2	6.47	3.86
Mg	I	382.94	0.90	3	5.95	14.84
Mg	I	516.73	0.11	3	5.11	5.99
Mg	I	517.27	0.34	3	5.11	17.96
Mg	I	518.36	0.56	3	5.11	24.04
Mg	**II**	**279.55**	**2.60**	**4**	**4.43**	**415.30**
Mg	II	280.27	2.57	2	4.42	208.03

Ca profile, as in both cases the distance to the shell border decreases for decreasing values of x.

4. Results and discussion

The analysis of the results derived from the two different laboratories clearly indicate that there are consistent similarities between the 2D Mg/Ca ratio maps obtained for the specimens under analysis. An initial comparison of the results obtained from the analysis of specimen LAN183 (collected in February) by the two groups is shown in Fig. 5.

Fig. 5 presents the analysis of specimen LAN183 performed by the two laboratories. Even if the spatial resolution delivered from the PEG setup is coarser (50 μm compared to 30 μm) the similarities derived from the resulting 2D maps are very similar, with 3 clear groups of growth portions with higher Mg/Ca concentrations (indicated as "organic-rich growth portions" in the figures and represented in lighter colors) to be found through the growth axis. These similarities can be also found on Fig. 5(b) and (d), where the evolution of the Mg/Ca profiles through the growth axis of the shell have been depicted following the path indicated by the black lines on Fig. 5(a) and (c). As expected, the profile associated with Fig. 5(d) is noisier, but in both cases cycles of seasonality can be observed, and there are clear similarities in their evolution, with a peak of high Mg/Ca ratio at x ≈ 0.5 mm and lower values associated with the shell edge.

It should be mentioned that vertical scales in these figures are different because the LIBS analysis at LEIZA is performed via the ratios of two emission lines (see Experimental setups and processing techniques), therefore the vertical axis is expressed in arbitrary units. As an implementation of the CF-LIBS method is used to obtain the Mg/Ca 2D maps, the vertical axis is expressed in this case in mmol/mol.

The results associated with the comparative analyses performed on two additional specimens LAN176 (collected in February) and LAN254 (collected in August) are presented in Fig. 6. Despite the different associated spatial resolutions, there are clear similarities between the 2D Mg/Ca maps obtained in the two laboratories. Fig. 6(a1) and (b1) show a Mg/Ca 2D map where two regions of growth portions with higher Mg/Ca ratios are clearly distinguishable: one at the middle section of the shell and the other close to the left edge. Fig. 6 (a2) and (b2) depict the evolution of the Mg/Ca ratio following the linear path indicated by the black lines crossing the associated 2D maps. The cycles of seasonality can be easily identified, with both profiles being again very similar.

The specimen LAN254 is analysed in Fig. 6(c) and (d). Again, the similarities that can be observed in the 2D maps represented in Fig. 6(c1) and (d1) are confirmed by the similar patterns of the associated linear profiles of Fig. 6(c2) and (d2).

To extend the analysis, Figs. 7 and 8 show the obtained 2D LIBS maps and linear evolution of the Mg/Ca ratios for specimens LAN229 (Fig. 7 (a) and (b), collected in June), LAN96 (Fig. 7(c) and (d), collected in November) and LAN259 (Fig. 8, collected in August).

Fig. 7 illustrates this issue by showing the results associated with specimens LAN229 and LAN96. LAN229 was collected in June (spring) and its corresponding Mg/Ca 2D maps show a clear resemblance with a group of growth lines and increments with higher Mg/Ca ratios at x ≈ 3 mm (from the shell edge). This can be appreciated in Fig. 7(b2), but the evolution of the associated linear profile is not so clear in Fig. 7 (a2). In the case of LAN96, it is difficult to find similarities in the 2D maps and, additionally, the cyclicity expressed by Fig. 7(c2) and (d2) seem to be different.

The results associated with the analysis of the anterior and posterior edges of specimen LAN259 at LEIZA are presented in Fig. 8. The resulting 2D maps and Mg/Ca profiles enable the identification of an abrupt change in the Mg/Ca composition (highlighted in the figure). This change could be attributed to a sudden growth stoppage that complicates the interpretation of the expected cyclicity.

Finally, Fig. 9 shows the 2D maps and Mg/Ca profiles associated with specimen LAN176, where again the groups of organic-rich growth portions enable a direct comparison of the 2D maps obtained at LEIZA and PEG and the resulting Mg/Ca profiles also show clear similarities., with also clear similarities obtained in the Mg/Ca profiles derived from the different linear paths described on the 2D maps. The 2D maps from LEIZA (Fig. 9(a1)) and PEG (Fig. 9(b1)) used different linear trajectories, resulting in slightly different Mg/Ca profiles over the shell's growth. Fig. 9(a2), (a3) and (a4) and 9(b2), (b3) and (b4) represent the evolution of the Mg/Ca ratio associated with trajectories deployed on the higher, middle and lower sections of the shell, respectively. It can be observed how the selection of the points at the shell edge of the trajectories generates different patterns in the evolution of the Mg/Ca ratios. In particular, Fig. 9(a2) (b2) and (higher trajectories) show a Mg/Ca profile whose edge points seem to indicate higher seawater temperatures; on the contrary, Fig. 9(a3–a4) and (b3–b4) show a similar evolution of their Mg/Ca profiles, with a clear cyclicity and Mg/Ca values close to the shell edge indicating lower temperatures. Among the different reasons that may explain these differences in the results, in this case this effect seems to be caused by a non-uniform growth of the shell across the growth edge.

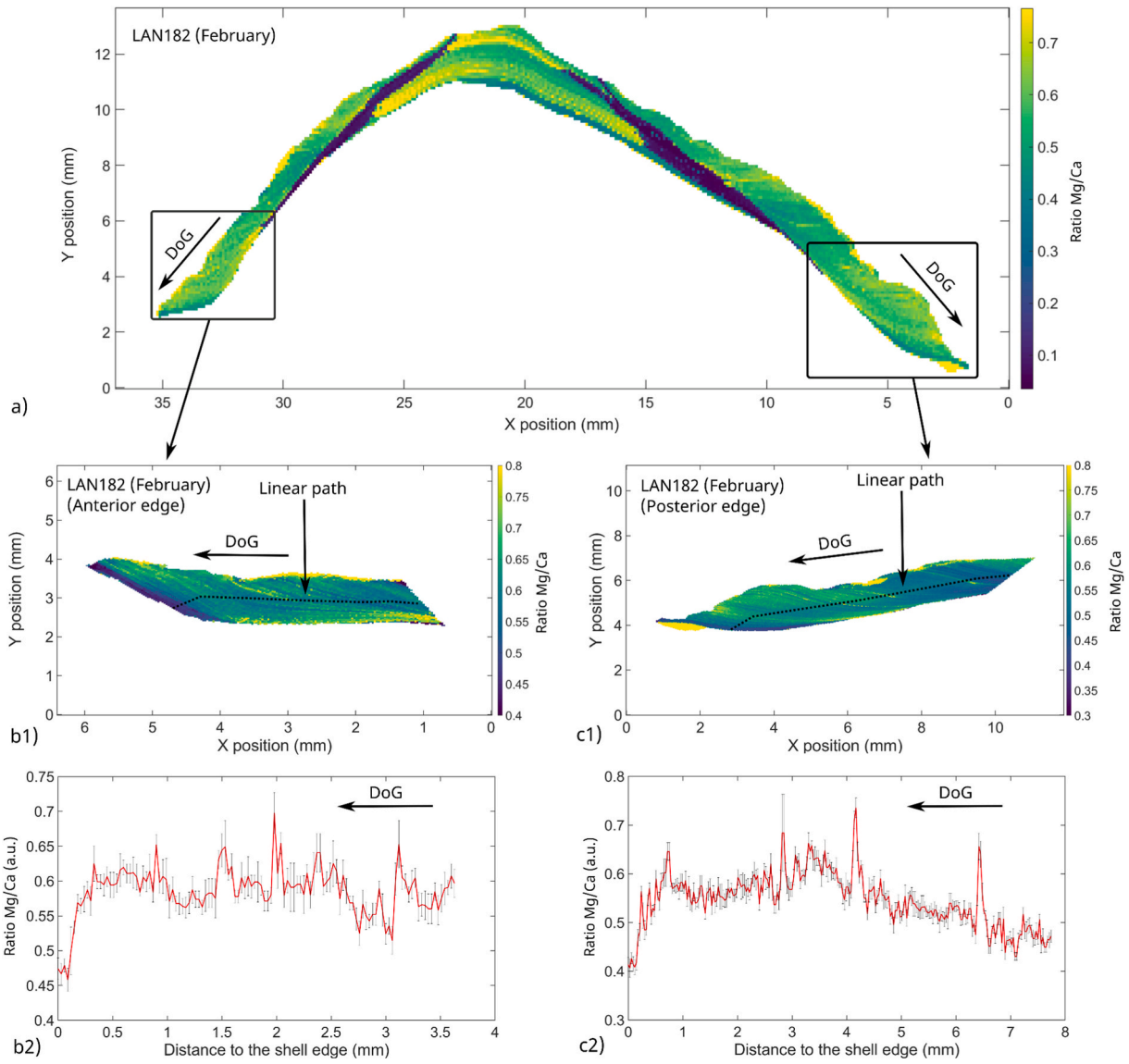

Fig. 4. (a) 2D LIBS map of the Mg/Ca ratio of specimen LAN182 obtained at LEIZA, using the ratio between the Mg II (279.553 nm) and Ca II (315.887 nm) emission lines, with a spatial resolution of 100 μm for the analysis of the whole section of the shell: (b1) Detail of 2D LIBS maps of the anterior edge of the shell (spatial resolution of 30 μm); (b2) Evolution of the Mg/Ca ratio through the growth axis of the shell associated with the 2D LIBS of the anterior edge; (c1) Detail of 2D LIBS maps of the posterior edge of the shell (spatial resolution of 30 μm); (c2) Evolution of the Mg/Ca ratio through the growth axis of the shell associated with the 2D LIBS of the posterior edge.

It is worth noting that the Mg/Ca values presented in this work are in good agreement with those reported in previous studies; both in terms of the Mg/Ca ratios obtained directly from the ratio of the chosen Ca II and Mg II emission lines [23,50] and the estimations made via CF-LIBS [6,25,28,37]. It must be also noted that, unlike CF-LIBS Mg/Ca estimations, raw line emission ratios are highly dependent on the spectral efficiency of the LIBS setup, plasma properties and other spectroscopic factors, so only relative values should be compared in experiments in different LIBS setups.

To complement the visual and descriptive comparison of the 2D Mg/Ca elemental maps generated by both laboratories, a quantitative similarity analysis was performed. For each specimen, the Structural Similarity Index (SSIM) [55] and the Pearson correlation coefficient [56] between the Mg/Ca maps obtained independently by the two laboratories were computed. SSIM provides a perceptual measure of image similarity by considering luminance, contrast, and structural information, while the Pearson coefficient quantifies the linear correlation between pixel intensity values.

Before the analysis, the images were resized to a common dimension to ensure compatibility. The results, presented in Table 4, show high SSIM values (ranging from 0.744 to 0.861) and strong Pearson correlations (0.660–0.780) across all specimens, with the only exception of LAN254, which shows slightly lower values (0.642 and 0.500, respectively). These values confirm a high degree of similarity between the maps, despite minor differences in resolution, orientation, and acquisition parameters. The quantitative analysis reinforces our conclusion that the elemental distribution patterns observed are highly reproducible across laboratories.

Although the two LIBS systems used in this study differ in several aspects, most notably in laser pulse duration, optical design, and processing techniques, these differences do not significantly affect the comparability of the 2D elemental maps generated. In fact, the use of two distinct systems adds value to the interlaboratory comparison, as it allows to evaluate the robustness of the results across different experimental configurations. It is acknowledged that such differences may influence the absolute intensity of the acquired emission lines, due to

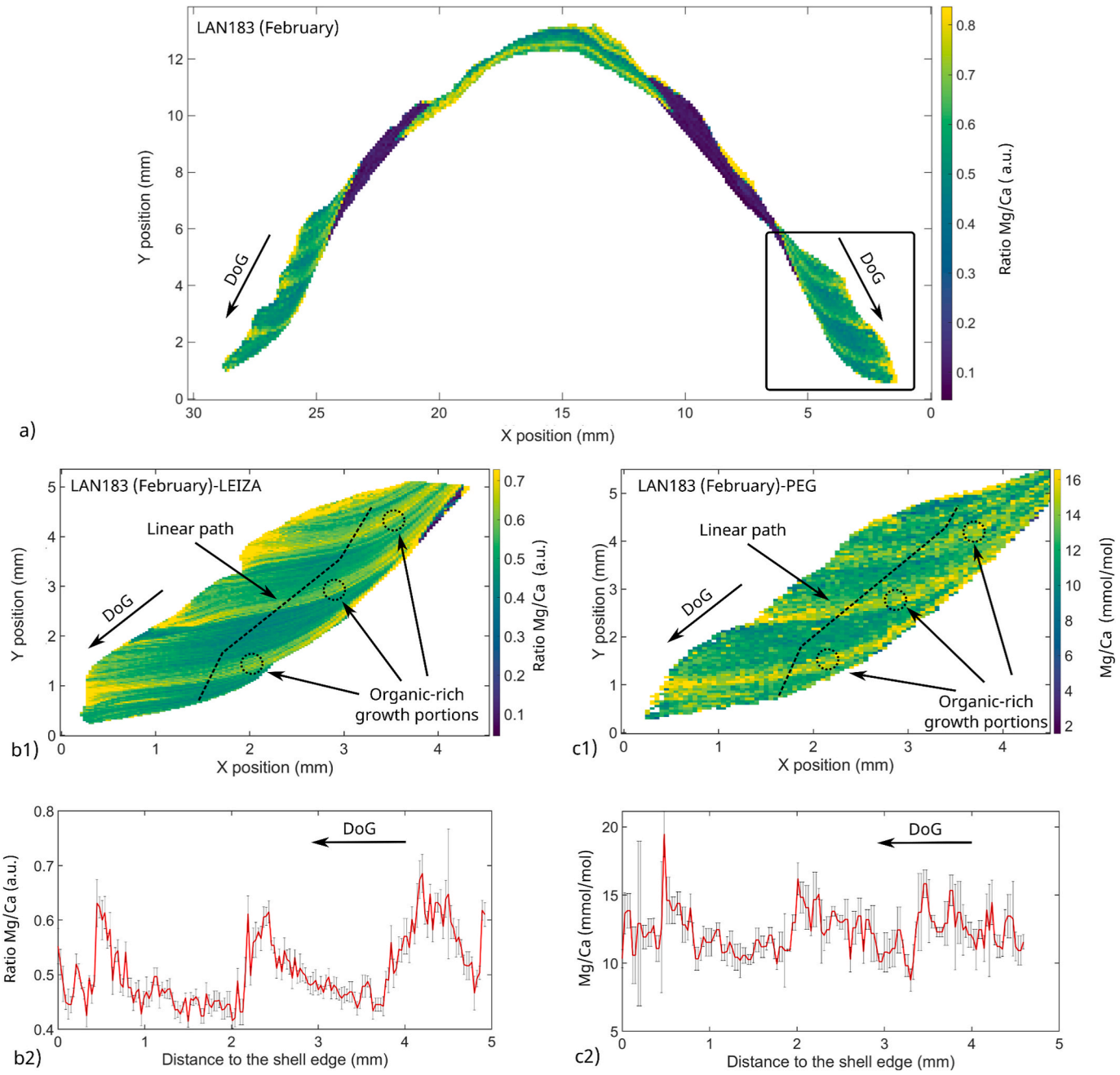

Fig. 5. 2D LIBS map of the Mg/Ca ratio of LAN183 (posterior edge) obtained at LEIZA and PEG: (a) 2D LIBS map of the Mg/Ca ratio obtained at LEIZA, using the ratio between the Mg II (279.553 nm) and Ca II (315.887 nm) emission lines, with a spatial resolution of 100 μm for the analysis of the whole section of the shell; (b1) detail of 2D LIBS maps of the posterior edge of the shell performed at LEIZA (spatial resolution of 30 μm); (b2) evolution of the Mg/Ca ratio through the growth axis of the shell associated with the 2D LIBS of the posterior edge (b1); (c1) detail of 2D LIBS map of the posterior edge of the shell performed at PEG (spatial resolution of 100 μm); (c2) evolution of the Mg/Ca ratio through the growth axis of the shell associated with the 2D LIBS of the posterior edge (c1).

variations in laser energy, spot size, ablation efficiency, and the spectral response of the optics and detectors involved. However, the processing techniques employed in both systems mitigate these effects. In one setup, elemental quantification is based on the ratio of two emission lines, which inherently compensates for intensity variations caused by system-specific optical or energy-related characteristics. In the other, the application of the CF-LIBS method further minimizes sensitivity to plasma or instrumental variability. Therefore, although the raw spectra differ between setups, the final 2D elemental maps are clearly comparable, as demonstrated by the results associated with the different specimens under analysis. The most relevant impact of the system differences lies in the spatial resolution of the elemental maps, driven by the distinct laser spot sizes, and in the total scanning time per specimen, with the higher laser repetition rate at LEIZA enabling significantly faster data acquisition.

These results indicate that LIBS is a suitable and efficient technique for the analysis of the 2D elemental composition of the shells. However, this efficiency does not necessarily imply that the technique offers a reliable estimation of the season of collection for all the studied specimens, which is out of the scope of this study.

It has been demonstrated that the different LIBS setups and processing techniques employed in this study offer similar results for the specimens under analysis. However, although Mg/Ca ratios have been widely employed as proxies for reconstructing past sea surface

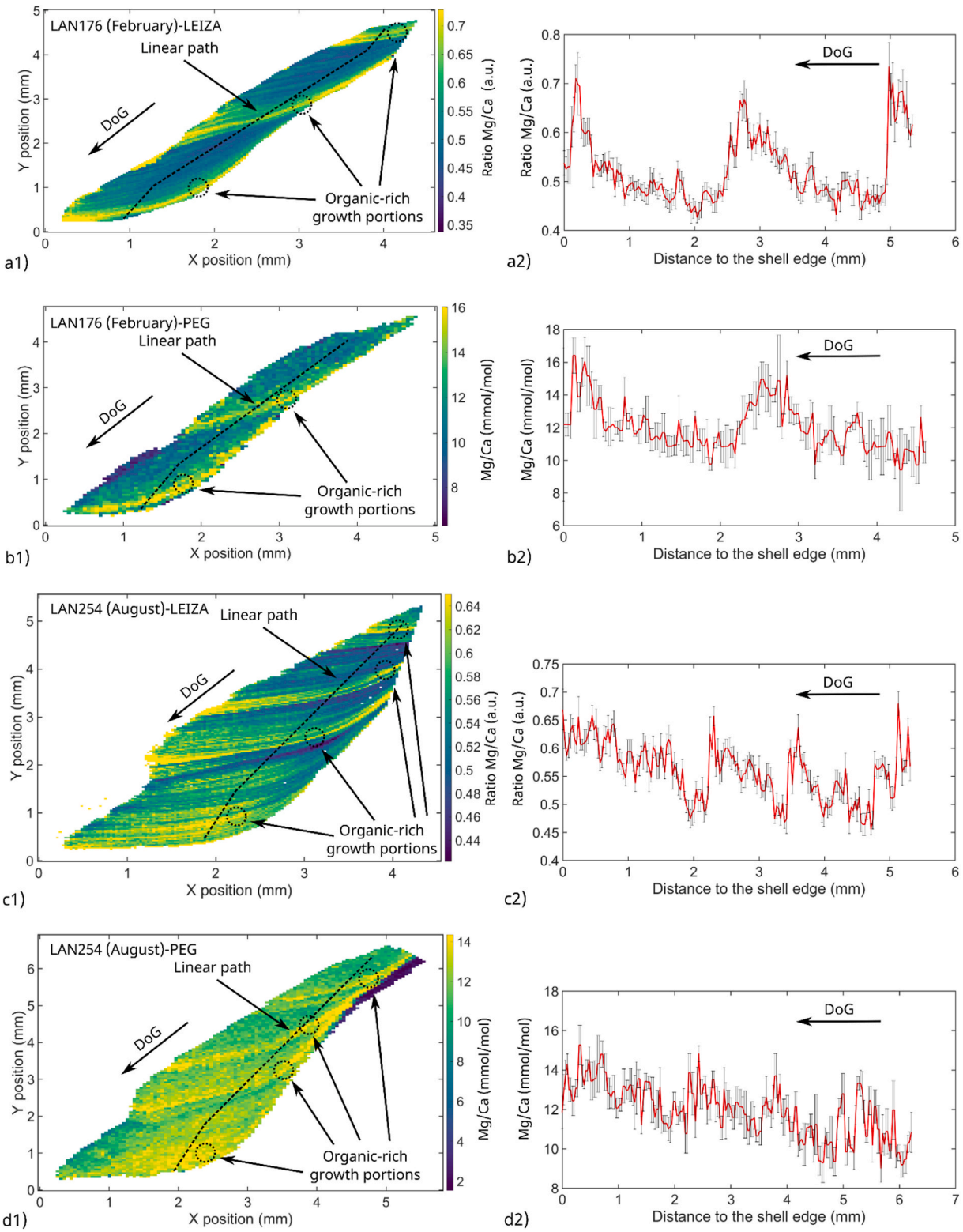

Fig. 6. Comparison of the 2D LIBS maps obtained at LEIZA and PEG: (a1–a2) 2D map and linear evolution of the Mg/Ca ratio for LAN176 analysed at LEIZA; (b1–b2) 2D map and linear evolution of the Mg/Ca ratio for LAN176 analysed at PEG; (c1–c2) 2D map and linear evolution of the Mg/Ca ratio for LAN254 analysed at LEIZA; (d1–d2) 2D map and linear evolution of the Mg/Ca ratio for LAN254 analysed at PEG.

temperatures (SST), several factors introduce limitations in their application for seasonal reconstructions. The SST [25] is not the only environmental factor affecting the final elemental composition of the shells. The impact of habitats within the same intertidal zone and the periods of time the limpets are submerged can influence the resulting Mg/Ca ratios [27]. Studies on specimens of the same species have revealed heterogeneous results regarding the chemical composition of shells. On the one hand, differences have been observed between shells from different locations. On the other hand, variability has also been found among specimens collected at the same site [6]. For example, Graniero et al.

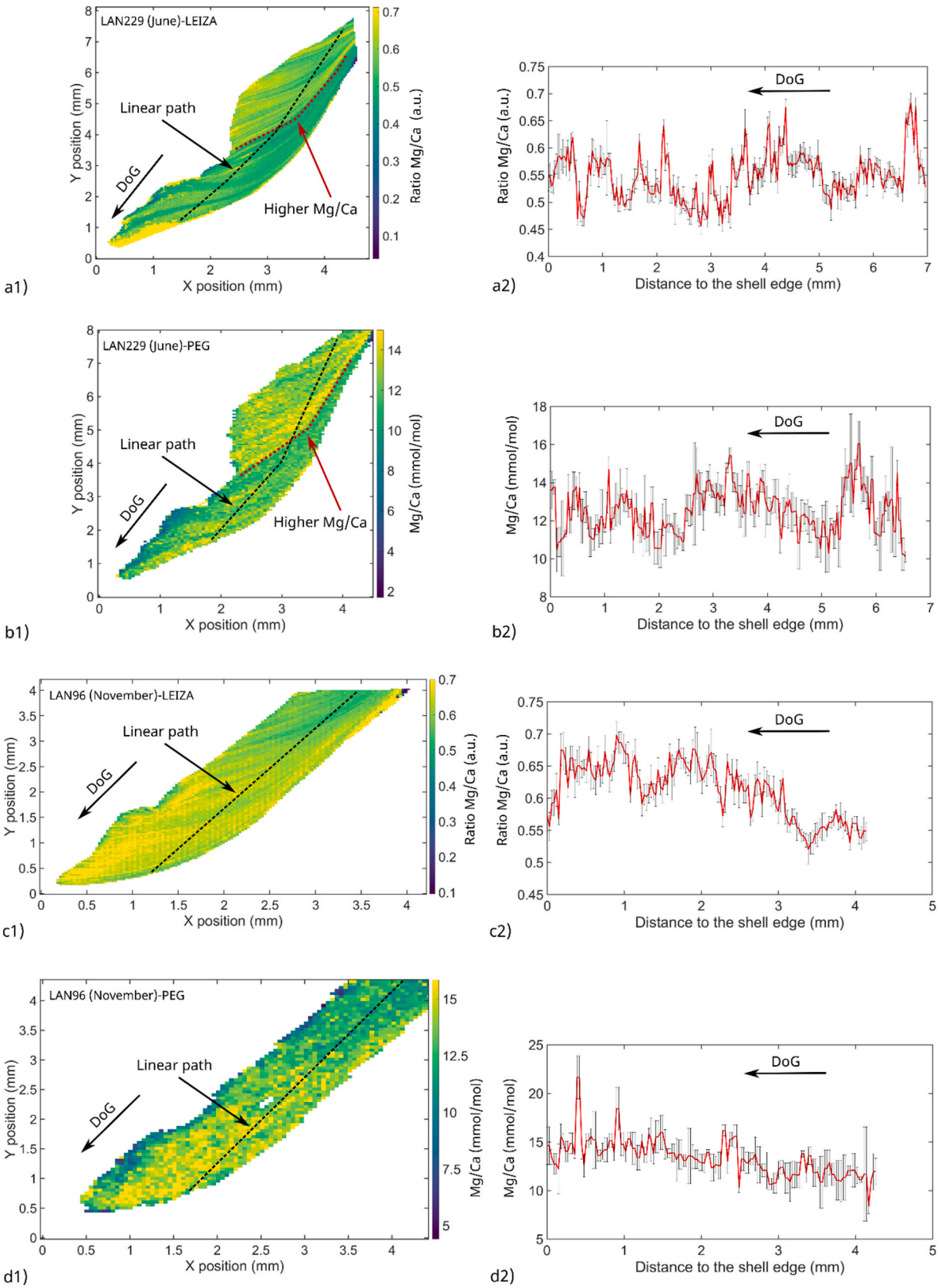

Fig. 7. Comparison of the 2D LIBS maps obtained at LEIZA and PEG: (a1–a2) 2D map and linear evolution of the Mg/Ca ratio for LAN229 analysed at LEIZA; (b1–b2) 2D map and linear evolution of the Mg/Ca ratio for LAN229 analysed at PEG; (c1–c2) 2D map and linear evolution of the Mg/Ca ratio for LAN96 analysed at LEIZA; (d1–d2) 2D map and linear evolution of the Mg/Ca ratio for LAN96 analysed at PEG.

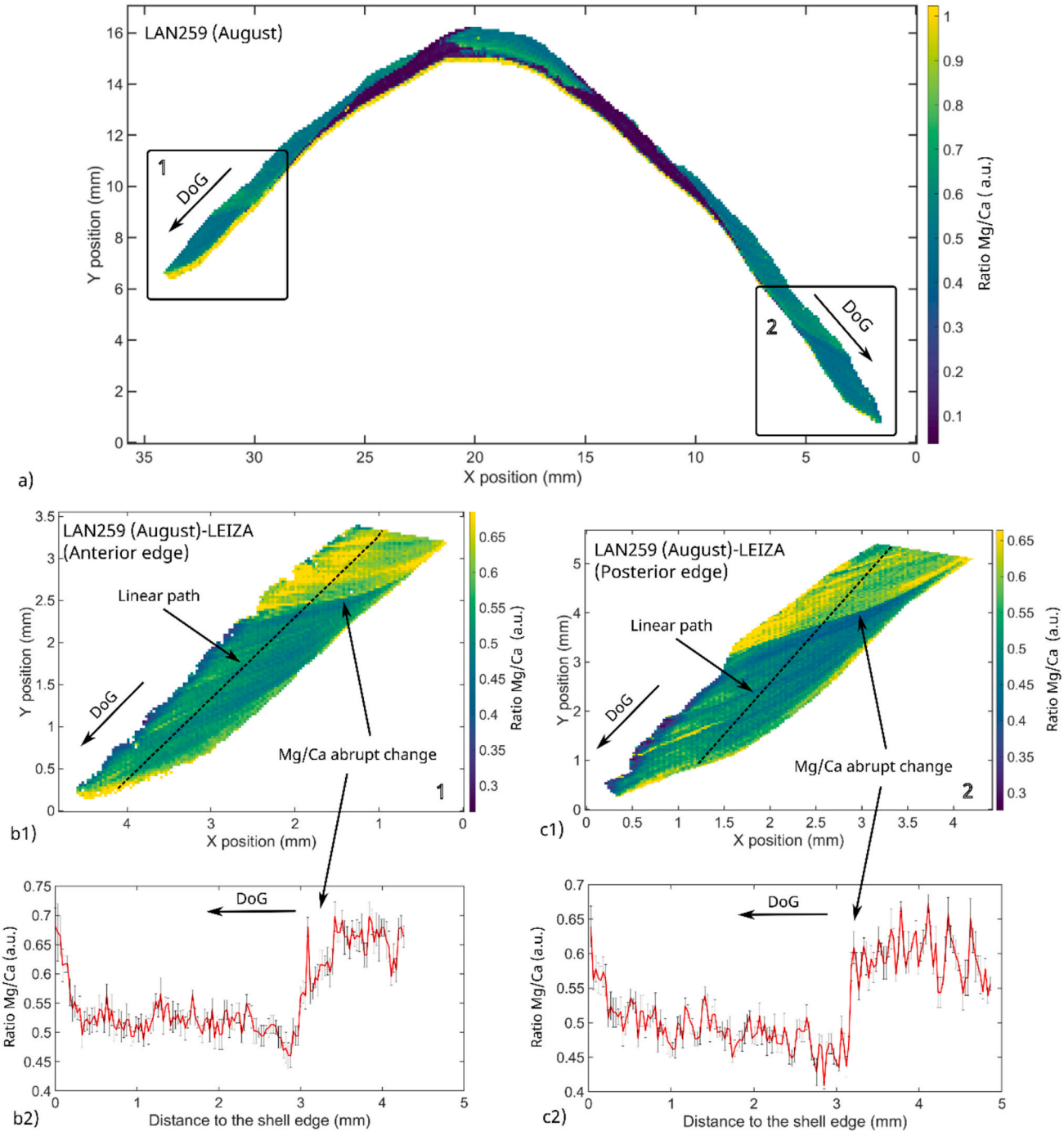

Fig. 8. Mg/Ca 2D map analysis of specimen LAN259 performed at LEIZA: (a1) Mg/Ca 2D map analysis of LAN259 (anterior edge); (a2) evolution of the Mg/Ca profile for LAN259 (anterior edge); (b1) Mg/Ca 2D map analysis of LAN259 (posterior edge); (b2) evolution of the Mg/Ca profile for LAN259 (posterior edge).

[54] documented significant differences in patelloid limpets from the North Sea (United Kingdom) and the Pacific Ocean (Tierra del Fuego). In contrast, Hausmann et al.'s studies on *P. caerulea* from the Mediterranean basin (Libya and Croatia) showed greater variability among specimens from the same location than between those from different locations [23].

The internal biological processes of these organisms significantly influence the composition at both the inter- and intraspecific levels [34]. The chemical variability in the growth layers within an individual can be attributed to characteristics of the inner crystal structure of the shell, such as crystal size and orientation [25,35,36]. It has been observed that Mg/Ca ratios gradually increase towards the shell's outer layer (m + 3) [27]. Furthermore, it is important to note that the Mg/Ca ratios in the annual growth lines may rise due to their substantial organic content [16].

Additionally, as stated by Cudennec *et al.* [34], the growth behaviour of some limpets is not only affected by environmental factors such as SST, but also by competition among limpets and endogenous factors like

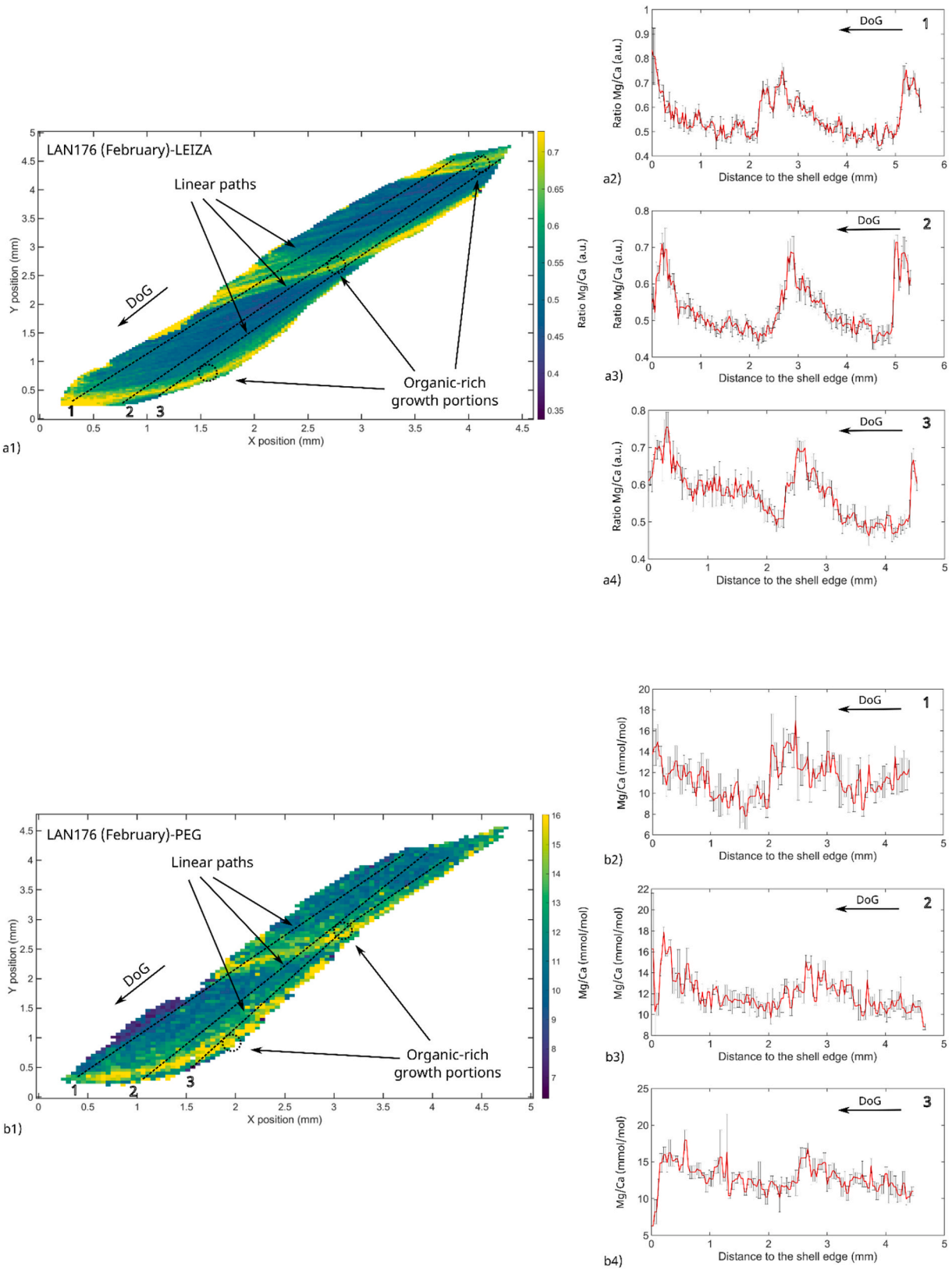

Fig. 9. Comparison of the Mg/Ca evolution profiles obtained for specimen LAN176 (analysed at LEIZA ((a) and PEG ((b)) for different trajectories represented in black dashed lines: (a1) 2D Mg/Ca map obtained at LEIZA; (a2) Mg/Ca profile associated with the trajectory deployed on the higher part of the shell; (a3) Mg/Ca profile associated with the trajectory deployed on the middle part of the shell; (a4) Mg/Ca profile associated with the trajectory deployed on the lower part of the shell; (b1) 2D Mg/Ca map obtained at PEG; (b2) Mg/Ca profile associated with the trajectory deployed on the higher part of the shell; (b3) Mg/Ca profile associated with the trajectory deployed on the middle part of the shell; (b4) Mg/Ca profile associated with the trajectory deployed on the lower part of the shell. Error bars show the standard deviation in each spatial point, calculated from the measurements of the several laser shots.

Table 4
Similarity metrics for 2D Mg/Ca LIBS maps across laboratories.

Specimen	SSIM	Pearson Correlation Coefficient
LAN96	0.744	0.660
LAN176	0.861	0.750
LAN183	0.812	0.780
LAN254	0.642	0.500
LAN229	0.843	0.704

age and sex. *P. vulgata*, for example, exhibits significant variations in its life history characteristics, encompassing aspects such as recruitment, growth, maximum size, and lifespan [34,57]. Although the primary focus of this study is on the comparison of 2D LIBS-derived elemental maps between laboratories, we acknowledge that environmental factors such as sea surface temperature (SST), salinity, and habitat conditions can significantly influence Mg/Ca ratios in mollusc shells. The interpretation of these ratios is further complicated by the potential interplay of environmental and endogenous factors. While the present work does not aim to quantify the contribution of these environmental variables, other studies have explored these relationships in more depth [27,29,54,61]. These investigations have used statistical approaches to assess the correlation between Mg/Ca ratios and SST in Patella and other marine mollusc species. Future work could benefit from combining the robust elemental mapping strategies presented here with detailed environmental monitoring to enhance our understanding of these influences.

In addition to these environmental and endogenous factors, biological aspects such as the health status and genetic variability of individual organisms may also influence the elemental composition of mollusc shells. Stress-related physiological responses, for instance, have been associated with increased metabolic activity that can alter trace element incorporation into the shell, potentially affecting Mg/Ca and Sr/Ca ratios [58]. Furthermore, genetic differences can modulate the biomineralization process itself [59], as demonstrated by transcriptomic studies showing variable expression of genes involved in shell formation among individuals [60]. Although these aspects are beyond the scope of the present methodological study, they represent important sources of intra-specimen variability that should be considered in future research. In a recent study, Schöne *et al.* discussed the difficulties in interpreting the element/Ca ratios of bivalve shells, mentioning non-lattice bound and microstructure-specific element content as additional causes [61]. It is important to point out that, regarding crystallographic considerations, our analyses specifically targeted the m + 2 layer of modern limpet shells, whose structure is expected to be relatively homogeneous. Given that the shells studied are from recent, healthy specimens, significant chemical alterations or anomalies at the microscopic scale are not anticipated.

Within this scenario, the use of the Mg/Ca ratios to enable an unambiguous interpretation of the associated data for archaeological research gives rise to some relevant challenges. For example, in terms of the specimens under analysis in this work, an abrupt change in the Mg/Ca profiles has been detected in two cases (LAN184, LAN259), which complicates the analysis. The results obtained for LAN259 at LEIZA are presented in Fig. 8, where an abrupt change in the Mg/Ca ratio at x $\approx$ 3 mm from the shell edge can be observed. A possible explanation for this behaviour is a sudden stoppage in the shell growth for an extended period of time. Previous studies have indicated the relevance of the identification of periods of growth cessation/slowdown for the correct interpretation of the season of collection [45].

Therefore, while Mg/Ca ratios can provide valuable palaeoclimatic insights, their application for seasonal reconstructions requires careful consideration of these limitations and, where possible, complementary validation with other proxies such as $\delta^{18}O$ measurements. A recent study has shown very good correlations for Mg/Ca concentrations and SST for P. vulgata, N. deaurata, and N. magellanica by using information derived from 2D LIBS maps and dynamic time warping [61].

5. Conclusions

In this work we obtained results using two different LIBS systems for the elemental analysis of mollusc shells. In particular, 20 specimens of *P. vulgata* have been analysed and their Mg/Ca 2D maps have been obtained. By comparing the results derived from both laboratories, it has been demonstrated that there is a high level of similarity between the 2D maps associated with each specimen. In this way, it can be concluded that some of the inaccuracies and anomalous data typically found during elemental sclerochronological analyses are not all dependent on the specific implementation of the LIBS setup or the chosen parameters, but derived from causes related to the mollusc shell specimens themselves, such as endogenous factors or competition among limpets. In terms of the comparison between the obtained 2D maps, the only specimen (LAN96) that do not present a high similarity is associated with Mg/Ca 2D maps where no clear growth lines or increments with high Mg/Ca ratios can be distinguished. This makes it more complicated to establish a fair comparison between the maps.

Within this context, it is well known that LIBS offers some advantages in comparison to other techniques enabling alternative climate proxies, such as a fast analysis (a few minutes for linear trajectories, minutes to a few hours for complete 2D maps) and minimum preparation of the samples. Additionally, the use of the 2D mapping procedure enables a more complete analysis of the Mg/Ca ratios of the shells, as the traditional 1D single trajectory mapping could give rise to some problems. For example, the shell edge under analysis does not always present a constant Mg/Ca ratio though the isochronous growth lines and increments, which can give rise to different results in the estimation of the season of collection depending on the final points chosen for the LIBS mapping trajectory. However, it seems clear that the selection of the 1D trajectory on the shell is key to obtain a suitable evolution of the Mg/Ca profiles, which can subsequently be used for correlation tests with other geochemical proxies such as $\delta^{18}O$.

In summary, in this work we demonstrated the following:

- The consistency of 2D elemental mapping using different LIBS systems and techniques (Mg/Ca ratio vs. CF-LIBS).
- Data anomalies do not originate from the analytical LIBS systems, but from the sample material itself.
- There is potential for future data processing techniques to further evaluate and critically assess 2D maps of mollusc shells.

To further advance LIBS-based elemental imaging, refining data processing techniques should be a priority. In particular, future efforts should focus on developing algorithms capable of directly interpreting 2D Mg/Ca maps to identify seasonal cycles and estimate the season of collection. This could include the application of automated pattern recognition methods, image segmentation, or machine learning models trained to detect characteristic growth features. Such tools would improve the objectivity, reproducibility, and analytical utility of LIBS in both archaeological and palaeoclimate research. It would also prove interesting to use the 2D maps to try to find a metric able to identify specimens that might be problematic in terms of the estimation of their corresponding seasons of collection and, ultimately, to find out the underlying cause (e.g. growth stops). Additionally, this study will be extended to other mollusc species and will consider the use of additional techniques such as Transmission Electron Microscopy (TEM) and Atom Probe Tomography (APT) to investigate the individual differences in the internal microscopic structure and elemental distribution of shells. The consistency of the 2D Mg/Ca LIBS maps between the two laboratories has been demonstrated, but the fact that all specimens originated from a single location may limit the broader generalization of the findings. To broaden the applicability of our conclusions, future work will also aim to include specimens collected from different geographical regions,

allowing us to assess the consistency of LIBS-derived elemental patterns across varying environmental and ecological conditions.

The ability of LIBS to generate high-resolution 2D elemental maps has significant implications for both archaeological and climate studies. From a palaeoclimatic perspective, the improved spatial resolution and mapping consistency enable a more detailed reconstruction of seasonal sea surface temperature variations, particularly when combined with other geochemical proxies. A recent study demonstrates that the use of the elemental information stored in the growth increments of the shell significantly improves the resulting Mg/Ca profiles, enabling a better interpretation of the seasonality [37]. In archaeology, the ability to detect subtle growth interruptions or seasonal signals in mollusc shells can provide insights into harvesting practices, site seasonality, and past human-environment interactions. These applications are particularly relevant in regions where molluscs were a key subsistence resource and where fine-scale environmental data can enrich cultural interpretations.

Future improvements in LIBS methodology should focus on standardizing experimental parameters across different setups and developing calibration protocols to mitigate matrix effects and laser-material interaction variability. Notably, our results demonstrate that, even when using different LIBS systems and parameters, the obtained 2D Mg/Ca maps exhibit remarkable similarity, confirming the technique's robustness and reliability across varied implementations.

CRediT authorship contribution statement

Jesús Mirapeix: Writing – review & editing, Writing – original draft, Visualization, Investigation, Formal analysis, Data curation. **Rosa Arniz-Mateos:** Writing – review & editing, Visualization, Resources, Investigation, Formal analysis, Data curation. **Danai Theodoraki:** Software, Methodology, Investigation, Formal analysis, Data curation. **Asier García-Escárzaga:** Writing – review & editing, Validation, Supervision, Resources, Methodology, Investigation, Funding acquisition, Formal analysis. **Víctor Piñon:** Writing – review & editing, Software, Investigation. **Igor Gutierrez-Zugasti:** Writing – review & editing, Validation, Supervision, Resources, Project administration, Funding acquisition. **Niklas Hausmann:** Writing – review & editing, Validation, Supervision, Project administration, Methodology, Investigation, Funding acquisition, Formal analysis, Conceptualization. **Adolfo Cobo:** Writing – review & editing, Software, Project administration, Investigation, Funding acquisition, Formal analysis, Data curation, Conceptualization.

Declaration of competing interest

The authors declare that they have no known competing financial interests or personal relationships that could have appeared to influence the work reported in this paper.

Acknowledgements

This research was supported by grant PID2021-124059NB-I00 funded by MICIU/AEI/10.13039/501100011033 and by FEDER, UE. RAM was supported by a predoctoral grant "Concepción Arenal" (grant number: 2019-8461) in the University of Cantabria during the development of this research. During the development of this research AGE was funded by the Catalonia Postdoctoral Programme through a Beatriu de Pinós fellowship (2020_BP_00240) and he is currently working in the framework of a Marie Skłodowska Curie Action – Postdoctoral Fellowship (101064225-NEARCOAST, https://doi.org/10.3030/101064225), funded by the European Commission. NH and DT acknowledge funding from the German Research Foundation (DFG) under the Emmy Noether Programme (project number: 439799406).

Author's contribution

We confirm that all authors have approved the final version of the manuscript and have made substantial contributions. All authors interpreted the data. All authors wrote and provided comments on the manuscript. RAM and JM carried out the data acquisition.

Declaration of generative AI and AI-assisted technologies in the writing process

During the preparation of this work the authors used ChatGPT (OpenAI) as a writing assistant to support the grammatical revision and refinement of the manuscript. After using this tool/service, the authors reviewed and edited the content as needed and take full responsibility for the content of the publication.

Data availability

Data will be made available on request.

References

[1] B.R. Schöne, The curse of physiology—challenges and opportunities in the interpretation of geochemical data from mollusk shells, Geo-Mar. Lett. 28 (2008) 269–285.
[2] N.J. Shackleton, Oxygen isotope analysis as a means of determining season of occupation of prehistoric midden sites, Archaeometry 15 (1) (1973) 133–141.
[3] S. Epstein, R. Buchsbaum, H.A. Lowenstam, H.C. Urey, Revised carbonate-water isotopic temperature scale, Geol. Soc. Am. Bull. 64 (11) (1953) 1315–1326.
[4] E.L. Grossman, T.L. Ku, Oxygen and carbon isotope fractionation in biogenic aragonite: temperature effects, Chem. Geol. Isot. Geosci. Sect. 59 (C) (1986) 59–74.
[5] B.R. Schöne, D.P. Gillikin, Unraveling environmental histories from skeletal diaries—advances in sclerochronology, Palaeogeogr. Palaeoclimatol. Palaeoecol. 373 (2013) 1–5.
[6] J.E. Ferguson, G.M. Henderson, D.A. Fa, J.C. Finlayson, N.R. Charnley, Increased seasonality in the Western Mediterranean during the last glacial from limpet shell geochemistry, Earth Planet. Sci. Lett. 308 (3–4) (2011) 325–333.
[7] A.D. Wanamaker, K.J. Kreutz, B.R. Schöne, N. Pettigrew, H.W. Borns, D.S. Introne, D. Belknap, K.A. Maasch, S. Feindel, Coupled North Atlantic slope water forcing on Gulf of Maine temperatures over the past millennium, Clim. Dyn. 31 (2008) 183–194.
[8] T. Wang, D. Surge, S. Mithen, Seasonal temperature variability of the Neoglacial (3300–2500 BP) and Roman Warm Period (2500–1600 BP) reconstructed from oxygen isotope ratios of limpet shells (Patella vulgata), Northwest Scotland, Palaeogeogr. Palaeoclimatol. Palaeoecol. 317 (2012) 104–113.
[9] C.F.T. Andrus, Shell midden sclerochronology, Quat. Sci. Rev. 30 (21–22) (2011) 2892–2905.
[10] C.F. West, M. Burchell, C.F.T. Andrus, Molluscs and paleoenvironmental reconstruction in island and coastal settings: variability, seasonality, and sampling, in: Zooarchaeology in Practice: Case Studies in Methodology and Interpretation in Archaeofaunal Analysis, 2018, pp. 191–208.
[11] A.D. Wanamaker Jr., K.J. Kreutz, T. Wilson, H.W. Borns Jr., D.S. Introne, S. Feindel, Experimentally determined Mg/Ca and Sr/Ca ratios in juvenile bivalve calcite for Mytilus edulis: implications for paleotemperature reconstructions, Geo Mar. Lett. 28 (5–6) (2008) 359–368.
[12] C. Poulain, D.P. Gillikin, J. Thebault, J.-M. Munaron, M. Bohn, R. Robert, Y.-M. Paulet, A. Lorrain, An evaluation of Mg/Ca, Sr/Ca, and Ba/Ca ratios as environmental proxies in aragonite bivalve shells, Chem. Geol. 396 (2015) 42–50.
[13] C. Brosset, N. Höche, R. Witbaard, K. Nishida, K. Shirai, R. Mertz-Kraus, B. R. Schöne, Sr/Ca in shells of laboratory-grown bivalves (Arctica islandica) serves as a proxy for water temperature–implications for (paleo) environmental research? Front. Mar. Sci. (2023).
[14] S.R. Durham, D.P. Gillikin, D.H. Goodwin, G.P. Dietl, Rapid determination of oyster lifespans and growth rates using LA-ICP-MS line scans of shell Mg/Ca ratios, Palaeogeogr. Palaeoclimatol. Palaeoecol. 485 (2017) 201–209.
[15] A. Barats, C. Pécheyran, D. Amouroux, S. Dubascoux, L. Chauvaud, O.F.X. Donard, Matrix-matched quantitative analysis of trace-elements in calcium carbonate shells by laser-ablation ICP–MS: application to the determination of daily scale profiles in scallop shell (Pecten maximus), Anal. Bioanal. Chem. 387 (2007) 1131–1140.
[16] B.R. Schoene, Z. Zhang, D. Jacob, D.P. Gillikin, T. Tütken, D. Garbe-Schönberg, A. Soldati, Effect of organic matrices on the determination of the trace element chemistry (Mg, Sr, Mg/Ca, Sr/Ca) of aragonitic bivalve shells (Arctica islandica)—comparison of ICP-OES and LA-ICP-MS data, Geochem. J. 44 (1) (2010) 23–37.
[17] P.S. Freitas, L.J. Clarke, H. Kennedy, C.A. Richardson, The potential of combined Mg/Ca and δ18O measurements within the shell of the bivalve Pecten maximus to estimate seawater δ18O composition, Chem. Geol. 291 (2012) 286–293.
[18] A. García-Escárzaga, I. Gutiérrez-Zugasti, A.B. Marín-Arroyo, R. Fernandes, S. Núñez de la Fuente, D. Cuenca-Solana, E. Iriarte, C. Simoes, J. Martin-Chivelet,

M.R. Gonzalez-Morales, P. Roberts, Human forager response to abrupt climate change at 8.2 ka on the Atlantic coast of Europe, Sci. Rep. 12 (1) (2022) 6481.
[19] N. Hausmann, M. Meredith-Williams, Seasonal patterns of coastal exploitation on the Farasan Islands, Saudi Arabia, J. Island Coast. Archaeol. 12 (3) (2017) 360–379.
[20] K.D. Thomas, Molluscs emergent, Part I: themes and trends in the scientific investigation of mollusc shells as resources for archaeological research, J. Archaeol. Sci. 56 (2015) 133–140.
[21] A.C. Colonese, G. Zanchetta, A.E. Fallick, R. Drysdale, Late Pleistocene-Holocene climate transition in the western Mediterranean: a view from the stable isotopes of land snail shells, Black Sea/Mediterranean Environ. 78 (2014).
[22] M. Stephens, D. Mattey, D.D. Gilbertson, C.V. Murray-Wallace, Shell-gathering from mangroves and the seasonality of the Southeast Asian Monsoon using high-resolution stable isotopic analysis of the tropical estuarine bivalve (Geloina erosa) from the Great Cave of Niah, Sarawak: methods and reconnaissance of molluscs of early Holocene and modern times, J. Archaeol. Sci. 35 (10) (2008) 2686–2697.
[23] N. Hausmann, D. Theodoraki, V. Piñon, P. Siozos, A. Lemonis, D. Anglos, Applying laser induced breakdown spectroscopy (LIBS) and elemental imaging on marine shells for archaeological and environmental research, Sci. Rep. 13 (1) (2023) 19812.
[24] A. García-Escárzaga, S. Moncayo, I. Gutiérrez-Zugasti, M.R. González-Morales, J. Martín-Chivelet, J.O. Cáceres, Mg/Ca ratios measured by laser induced breakdown spectroscopy (LIBS): a new approach to decipher environmental conditions, J. Anal. At. Spectrom 30 (9) (2015) 1913–1919.
[25] A. Cobo, A. García-Escárzaga, I. Gutiérrez-Zugasti, J. Setién, M.R. González-Morales, J.M. López-Higuera, Automated measurement of magnesium/calcium ratios in gastropod shells using laser-induced breakdown spectroscopy for paleoclimatic applications, Appl. Spectrosc. 71 (4) (2017) 591–599.
[26] A. García-Escárzaga, L.J. Clarke, I. Gutiérrez-Zugasti, M.R. González-Morales, M. Martinez, J.M. López-Higuera, A. Cobo, Mg/Ca profiles within archaeological mollusc (Patella vulgata) shells: Laser-induced breakdown spectroscopy compared to inductively coupled plasma-optical emission spectrometry, Spectrochim. Acta B At. Spectrosc. 148 (2018) 8–15.
[27] N. Hausmann, A.L. Prendergast, A. Lemonis, J. Zech, P. Roberts, P. Siozos, D. Anglos, Extensive elemental mapping unlocks Mg/Ca ratios as climate proxy in seasonal records of Mediterranean limpets, Sci. Rep. 9 (1) (2019) 3698.
[28] M. Martínez-Minchero, A. Cobo, A. Méndez-Vicente, J. Pisonero, N. Bordel, I. Gutiérrez-Zugasti, P. Roberts, A. Arrizabalaga, J. Valdiande, J. Mirapeix, J. M. Lopez-Higuera, A. García-Escárzaga, Comparison of Mg/Ca concentration series from Patella depressa limpet shells using CF-LIBS and LA-ICP-MS, Talanta 251 (2023) 123757.
[29] A. García-Escárzaga, M. Martínez-Minchero, A. Cobo, I. Gutiérrez-Zugasti, A. Arrizabalaga, P. Roberts, Using Mg/Ca ratios from the limpet Patella depressa Pennant, 1777 measured by laser-induced breakdown spectroscopy (LIBS) to reconstruct paleoclimate, Appl. Sci. 11 (7) (2021) 2959.
[30] Y. Li, Y. Wang, S. Wang, R. Zheng, Z. Bao, Y. Lu, Preliminary study of laser-induced breakdown spectroscopy for Mg/Ca investigation in cultured scallop shells, J. Laser Appl. 35 (2) (2023).
[31] Y. Lu, Y. Li, Y. Li, Y. Wang, S. Wang, Z. Bao, R. Zheng, Micro spatial analysis of seashell surface using laser-induced breakdown spectroscopy and Raman spectroscopy, Spectrochim. Acta B At. Spectrosc. 110 (2015) 63–69.
[32] N. Hausmann, P. Siozos, A. Lemonis, A.C. Colonese, H.K. Robson, D. Anglos, Elemental mapping of Mg/Ca intensity ratios in marine mollusc shells using laser-induced breakdown spectroscopy, J. Anal. At. Spectrom 32 (8) (2017) 1467–1472.
[33] Y. Li, Y. Lu, Y. Lan, Y. Li, J. Guo, R. Zheng, Sr/Ca ratio analysis of seashells using laser-induced breakdown spectroscopy under objective-lens focusing and single-lens focusing, Appl. Opt. 57 (13) (2018) 3539–3545.
[34] J.F. Cudennec, Y.M. Paulet, Characterizing inter-individual growth variability of Patella vulgata shell through calcein marking experiments: consequences for palaeo-environmental studies, Environ. Archaeol. 27 (6) (2022) 525–538.
[35] C.E. Lazareth, F. Le Cornec, F. Candaudap, R. Freydier, Trace element heterogeneity along isochronous growth layers in bivalve shell: consequences for environmental reconstruction, Palaeogeogr. Palaeoclimatol. Palaeoecol. 373 (2013) 39–49.
[36] B.R. Schöne, P. Radermacher, Z. Zhang, D.E. Jacob, Crystal fabrics and element impurities (Sr/Ca, Mg/Ca, and Ba/Ca) in shells of Arctica islandica—implications for paleoclimate reconstructions, Palaeogeogr. Palaeoclimatol. Palaeoecol. 373 (2013) 50–59.
[37] J. Mirapeix, R. Arniz-Mateos, A. García-Escárzaga, I. Gutiérrez-Zugasti, J.M. López-Higuera, A. Cobo, Virtual sampling: archaeological implications of a new technique for elemental mapping of Mg/Ca ratios in marine mollusc shells, J. Archaeol. Sci. 173 (2025) 106123.
[38] V. Piñon, M.P. Mateo, G. Nicolas, Laser-induced breakdown spectroscopy for chemical mapping of materials, Appl. Spectrosc. Rev. 48 (5) (2013) 357–383.
[39] J.R. Chirinos, D.D. Oropeza, J.J. Gonzalez, H. Hou, M. Morey, V. Zorba, R.E. Russo, Simultaneous 3-dimensional elemental imaging with LIBS and LA-ICP-MS, J. Anal. At. Spectrom 29 (7) (2014) 1292–1298.
[40] C. Vander Pyl, O. Ovide, M. Ho, B. Yuksel, T. Trejos, Spectrochemical mapping using laser induced breakdown spectroscopy as a more objective approach to shooting distance determination, Spectrochim. Acta B At. Spectrosc. 152 (2019) 93–101.
[41] http://seafront-project.com/.
[42] G.T. Poppe, Y. Goto, European Seashells (polyplacophora, Caudofoveata, Solenogastra, Gastropoda) vol. I (1991) 1.
[43] T. Fenger, D. Surge, B. Schöne, N. Milner, Sclerochronology and geochemical variation in limpet shells (Patella vulgata): a new archive to reconstruct coastal sea surface temperature, Geochem. Geophys. Geosyst. 8 (7) (2007).
[44] P. Foster, J. Chacko, Minor and trace elements in the shell of Patella vulgata (L.), Mar. Environ. Res. 40 (1) (1995) 55–76.
[45] I. Gutiérrez-Zugasti, R. Suárez-Revilla, L. Clarke, B. Schöne, G. Bailey, M. Gonzalez Morales, Shell oxygen isotope values and sclerochronology of the limpet Patella vulgata Linnaeus 1758 from northern Iberia: Implications for the reconstruction of past seawater temperatures, Palaeogeogr. Palaeoclimatol. Palaeoecol. 484 (2017).
[46] A.S. Craighead, Marine mollusca as palaeoenvironmental and palaeoeconomic indicators in Cantabrian Spain, University of Cambridge, Cambridge, 1995. Unpublished doctoral dissertation.
[47] G.N. Bailey, A.S. Craighead, Late Pleistocene and Holocene coastal palaeoeconomies: a reconsideration of the molluscan evidence from northern Spain, Geoarchaeol.: Int. J. 18 (2) (2003) 175–204.
[48] https://physics.nist.gov/PhysRefData/ASD/Html/verhist.shtml.
[49] A. Ciucci, M. Corsi, V. Palleschi, S. Rastelli, A. Salvetti, E. Tognoni, New procedure for quantitative elemental analysis by laser-induced plasma spectroscopy, Appl. Spectrosc. 53 (8) (1999) 960–964.
[50] E. Tognoni, G. Cristoforetti, S. Legnaioli, V. Palleschi, Calibration-free laser-induced breakdown spectroscopy: state of the art, Spectrochim. Acta B At. Spectrosc. 65 (1) (2010) 1–14.
[51] E. Grifoni, S. Legnaioli, M. Lezzerini, G. Lorenzetti, S. Pagnotta, V. Palleschi, Extracting time-resolved information from time-integrated laser-induced breakdown spectra, J. Spectrosc. 2014 (1) (2014) 849310.
[52] F.U. Hongbo, N.I. Zhibo, W.A.N.G. Huadong, J.I.A. Junwei, D.O.N.G. Fengzhong, Accuracy improvement of calibration-free laser-induced breakdown spectroscopy, Plasma Sci. Technol. 21 (3) (2018) 034001.
[53] International Atomic Energy Agency, GENIE - General Internet Search Engine for Atomic Data, 2022. https://www-amdis.iaea.org/GENIE/.
[54] L.E. Graniero, D. Surge, D.P. Gillikin, I.B. i Godino, M. Álvarez, Assessing elemental ratios as a paleotemperature proxy in the calcite shells of patelloid limpets, Palaeogeogr. Palaeoclimatol. Palaeoecol. 465 (2017) 376–385.
[55] Z. Wang, A.C. Bovik, H.R. Sheikh, E.P. Simoncelli, Image quality assessment: from error visibility to structural similarity, IEEE Trans. Image Process. 13 (4) (2004) 600–612.
[56] G.W. Snedecor, W.G. Cochran, Statistical Methods, eighth edition, Iowa State University Press, 1989.
[57] J.R. Lewis, R.S. Bowman, Local habitat-induced variations in the population dynamics of Patella vulgata L. J. Exp. Mar. Biol. Ecol. 17 (2) (1975) 165–203.
[58] N. Schleinkofer, J. Raddatz, D. Evans, A. Gerdes, S. Flögel, S. Voigt, M. Wisshak, Compositional variability of Mg/Ca, Sr/Ca, and Na/Ca in the deep-sea bivalve Acesta excavata (Fabricius, 1779), PLoS One 16 (4) (2021) e0245605.
[59] H.L. Kempf, D.A. Gold, S.J. Carlson, Investigating the relationship between growth rate, shell morphology, and trace element composition of the pacific littleneck clam (Leukoma staminea): implications for paleoclimate reconstructions, Minerals 13 (6) (2023) 814.
[60] T. Yarra, K. Ramesh, M. Blaxter, A. Hüning, F. Melzner, M.S. Clark, Transcriptomic analysis of shell repair and biomineralization in the blue mussel, Mytilus edulis, BMC Genomics 22 (1) (2021) 437.
[61] B.R. Schöne, S. Marali, A. Jantschke, R. Mertz-Kraus, P.G. Butler, L. Fröhlich, Can element chemical impurities in aragonitic shells of marine bivalves serve as proxies for environmental variability? Chem. Geol. 616 (2023) 121215.
[62] N. Hausmann, D. Surge, I.B. i Godino, Confirmation of Mg/Ca ratios as palaeothermometers in Atlantic limpet shells, Palaeogeogr. Palaeoclimatol. Palaeoecol. 655 (2024) 112538.